Refraction Hall Effect

Ronika Sarkar, 1,2,* Arka Bandyopadhyay, 3,† Awadhesh Narayan, 2,‡ and Diptiman Sen^{4,§}

¹Department of Physics, Indian Institute of Science, Bangalore 560012, India
²Solid State and Structural Chemistry Unit, Indian Institute of Science, Bangalore 560012, India
³Institute for Theoretical Physics and Astrophysics, University of Würzburg, 97074 Würzburg, Germany
⁴Centre for High Energy Physics, Indian Institute of Science, Bangalore 560012, India

We introduce a new mechanism that produces a Hall-like response in time-reversal-invariant materials, driven entirely by geometric effects. Specifically, we demonstrate that a tilted potential interface causes electron wave packets to undergo a refraction-like deflection upon transmission through the barrier, leading to a finite transverse current and a corresponding Hall conductance. Our analytical framework captures the essential features of this *refraction Hall effect*, and the resulting Hall conductivity profile is corroborated by numerical simulations across different lattice models and device geometries. We further visualize our predicted effect through real-time wave packet dynamics, which reveals its purely geometric origin and the robustness of the transverse response. These findings establish a fundamentally distinct class of Hall-like transport phenomena in mesoscopic systems that preserve time-reversal symmetry.

Introduction- Transport phenomena at interfaces and the quantum Hall effect have long been central to our understanding of condensed matter systems and topological physics. Examples of interfaces include a junction between the surfaces of two topological insulators [1–3] and a junction between topological insulators and a superconductor [4]. Over the years, a variety of Hall effects have been identified, each revealing unique insights into the interplay between electron dynamics, external fields and material properties. Starting with the classical Hall effect [5], which describes the transverse voltage generated under an applied magnetic field, numerous related phenomena have been discovered. These include the anomalous Hall effect [6–8], where intrinsic spin-orbit coupling gives rise to a transverse charge current even without a magnetic field, and the spin Hall effect [9-13], which generates a transverse spin current in the absence of a charge current. In the quantum regime, extensive studies have focused on the integer and fractional quantum Hall effects [14–19], the quantum spin Hall effect [20-22], and the quantum anomalous Hall effect [23-25]. More recently, the thermal Hall effect [26–28] has attracted attention, linking temperature gradients to transverse currents, while additionally, non-linear Hall effects [29-32] have emerged as a new class of phenomena where the intrinsic Berry curvature dipole of a system leads to a second-order transverse response to external electric fields. Furthermore, the Magnus Hall effect [33-35] describes the generation of a linear transverse response in systems with an in-built electric field under inversion-symmetry breaking.

Although a vast body of research on Hall effects focuses on systems subject to magnetic fields, the possibility of generating transverse currents without breaking time-reversal symmetry remains relatively less explored. In this work, we investigate a geometric mechanism that induces a Hall-like response without using external magnetic or electric fields, arising from electron scattering at a tilted potential step. Using both analytical and numerical analyses under a small applied bias, we derive an expression for the differential Hall conductance and show that a transverse (Hall-like) current emerges due to angular refraction effects, reminiscent of optical refrac-

tion, which we term the refraction Hall effect.

We first analyze a single-electron case, where an electron refracts upon encountering a potential barrier at a fixed incidence angle, to compute the resulting Hall current. We then extend this to a biased device with a tilted potential interface, where electrons incident at arbitrary angles yield a Hall conductance dependent on the tilt angle and the potential strength. To further elucidate the dynamics, we simulate the time evolution of an electron wave packet in this geometry, visually illustrating the refraction-induced Hall response. Finally, we validate our theory through numerical simulations on square and hexagonal lattices, confirming the feasibility of the proposed effect in realistic experimental systems.

Electron refraction at a tilted potential interface—We begin

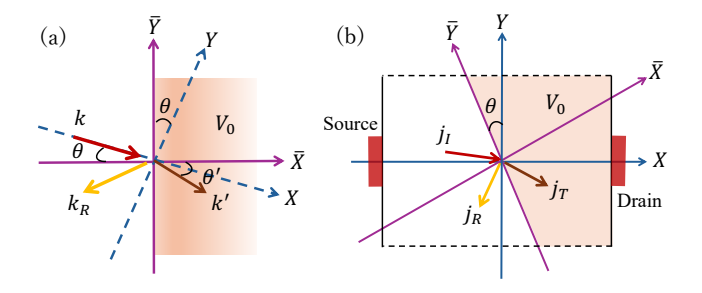


FIG. 1. Snell's law for electrons and schematic of the refraction Hall setup. (a) An electron with incident wavevector with magnitude k and angle θ impinges on a potential step aligned with the (\bar{X}, \bar{Y}) axes. Upon transmission, its wavevector changes to k' and the refracted trajectory emerges at an angle θ' , satisfying the conservation law $k \sin \theta = k' \sin \theta'$. (b) The device consists of a rectangular slab connected to a source and a drain along the X-axis and extending infinitely along Y. A potential barrier is engineered at an angle θ relative to the perpendicular axis (Y). The rotated coordinates (\bar{X}, \bar{Y}) follow the orientation of the barrier. The incident current density from the source, j_I , represents a single illustrative angle of incidence. The corresponding reflected and transmitted components are indicated by j_R and j_T , respectively, analogous to reflection and refraction in an optical setting.

by considering an electron with a wavevector of magnitude k incident at an angle θ on a potential step aligned with the Cartesian axes (\bar{X}, \bar{Y}) . Upon transmission into the region of constant potential V_0 , the electron experiences a refraction process directly analogous to Snell's law in optics [see Fig. 1(a)]. In this region, the wavevector magnitude changes to k', and the transmitted trajectory forms an angle θ' with the interface normal. Conservation of the parallel component of the wavevector leads to the relation, $k \sin \theta = k' \sin \theta'$.

In the context of our system depicted in Fig. 1(b), this configuration corresponds to an electron incident parallel to the sample from the source side, subsequently encountering the potential barrier at an angle θ . The electron dynamics is governed by the Schrödinger equation expressed in the (\bar{X}, \bar{Y}) coordinate system

$$\left[-\frac{\hbar^2}{2m} \nabla^2 + V(\bar{x}) \right] \psi(\bar{x}, \bar{y}) = E \psi(\bar{x}, \bar{y}). \tag{1}$$

The incident momenta components are $k_{\bar{x}}=\sqrt{\frac{2mE}{\hbar^2}}\cos\theta$ and $k_{\bar{y}}=\sqrt{\frac{2mE}{\hbar^2}}\sin\theta$, where E is the kinetic energy in region I (with zero potential). Due to the translational invariance along $\bar{Y},\ k_{\bar{y}}$ is conserved, and we employ the separable ansatz, $\psi(\bar{x},\bar{y})=\Phi(\bar{x})\chi(\bar{y})=\Phi(\bar{x})e^{ik_{\bar{y}}\bar{y}}$. The potential step exists at $\bar{x}=0$: $V(\bar{x})=0$ for $\bar{x}<0$ (region I) and $V(\bar{x})=V_0$ for $\bar{x}>0$ (region II). To proceed, we solve for the wavefunction separately in each region, which are given as, $\Phi_1(\bar{x})=e^{ik_x\bar{x}}+r\,e^{-ik_x\bar{x}},\ \Phi_2(\bar{x})=t\,e^{ik_x'\bar{x}},$ where, r and t denote the reflection and transmission coefficients, respectively, while k' represents the magnitude of the wavevector in the region with potential, defined as, $k'=\sqrt{\frac{2m(E-V_0)}{\hbar^2}}$. Specifically, translational invariance along \bar{Y} implies $k'_{\bar{y}}=k_{\bar{y}}$. Next, we evaluate the probability current, $J_{\alpha}=-\frac{i\hbar}{2m}(\psi^*\frac{\partial\psi}{\partial\alpha}-\psi\frac{\partial\psi^*}{\partial\alpha})$, in direction α . Applying this to region II, we obtain $J_{\bar{X}}=\frac{\hbar k'_{\bar{x}}}{m}|t|^2$, $J_{\bar{Y}}=\frac{\hbar k_{\bar{y}}}{m}|t|^2$. To estimate the Hall response, J_A , we calculate the cur-

To estimate the Hall response, J_A , we calculate the current density along the Y direction. The component of the current transverse to the sample can then be obtained, through a straightforward coordinate transformation, as

$$J_{A} = -J_{\bar{Y}}\cos\theta + J_{\bar{X}}\sin\theta$$

$$= \frac{\hbar}{m}|t|^{2}(-k_{\bar{y}}\cos\theta + k'_{\bar{x}}\sin\theta)$$

$$= \frac{\hbar}{m}|t|^{2}(-k\sin\theta\cos\theta + k'\cos\theta'\sin\theta).$$
(2)

By applying Snell's law of refraction, $k \sin \theta = k' \sin \theta'$, we can determine the angle of refraction θ' . Substituting the expressions for θ' and k' we obtain

$$J_A = |t|^2 \sqrt{\frac{2E}{m}} \sin \theta \left(-\cos \theta + \sqrt{\cos^2 \theta - \frac{V_0}{E}} \right). \quad (3)$$

Imposing the boundary conditions on ψ and its derivative $\frac{\partial \psi}{\partial \bar{x}}$ at $\bar{x}=0$, the transmission probability $|t|^2$ is determined

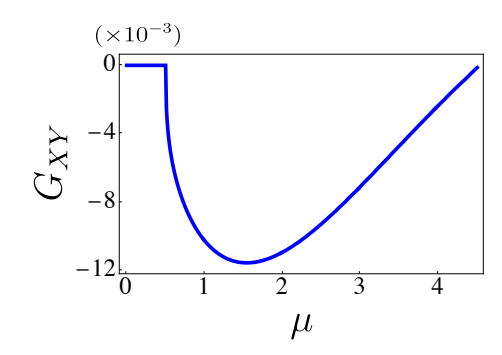


FIG. 2. Refraction Hall conductivity from analytical calculations. The calculated Hall conductivity, G_{XY} , is shown as a function of the Fermi energy μ . The parameters are fixed at a barrier strength $V_0=0.5$ and a tilt angle $\theta=0.025~\pi$. A finite Hall response emerges when the Fermi energy exceeds the barrier height V_0 . The conductivity is expressed in units of e^2/h .

as $t = \frac{2k_{\bar{x}}}{k_{\bar{x}} + k'_{\bar{x}}} = 2\left(1 + \sqrt{1 - \frac{V_0}{E\cos\theta}}\right)^{-1}$. Using these results, we arrive at the final expression for the Hall current in the single-electron case,

$$J_A = \sqrt{\frac{2E}{m}} \frac{4\sin\theta}{\left|1 + \sqrt{1 - \frac{V_0}{E\cos\theta}}\right|^2} \left(\sqrt{\cos^2\theta - \frac{V_0}{E}} - \cos\theta\right). \tag{4}$$

Two immediate consistency checks validate this expression. First, at zero tilt angle of the potential, the Hall response must vanish; this is satisfied as $J_A(\theta=0)=0$. Second, in the absence of a potential barrier, the response should vanish; this is also satisfied as $J_A(V_0=0)=0$.

The more physically relevant scenario corresponds to electrons incident at all possible angles, rather than a single electron incident at a specific angle. To address this case, we consider the system depicted in Fig. 1(b), which is finite along X and assumed to be infinite along Y. The sample is connected to a source and a drain along X, thus applying an external bias to the system. Furthermore, translational symmetry is preserved along \bar{Y} . As a result of the source, electrons may impinge on the potential barrier at a continuum of angles, and their collective contributions determine the net Hall response, if any. To analyze this, we recall the coordinate transformation to the device frame: $\hat{X} = \hat{X}\cos\theta - \hat{Y}\sin\theta$, $\hat{Y} = \hat{X}\sin\theta + \hat{Y}\cos\theta$, and focus on the response along \hat{Y} . For a single electron transmitted into the potential barrier, the corresponding current density is,

$$\delta I_Y = |t|^2 \frac{\hbar^2}{m} (k_{\bar{x}}' \sin \theta + k_{\bar{y}} \cos \theta). \tag{5}$$

Now, electrons may be incident at arbitrary angles, such that $k_{\bar{x}} = k\cos(\phi - \theta)$ and $k_{\bar{y}} = k\sin(\phi - \theta)$, where $\phi \in [-\frac{\pi}{2}, \frac{\pi}{2}]$. The source is assumed to supply a chemical potential $\mu_S = \mu + \delta \mu$, while the drain is held at $\mu_D = \mu$. Consequently, the electronic energies are constrained by the chemical potentials, such that, $\frac{2m\mu}{\hbar^2} < k^2 < \frac{2m(\mu + \delta \mu)}{\hbar^2}$.

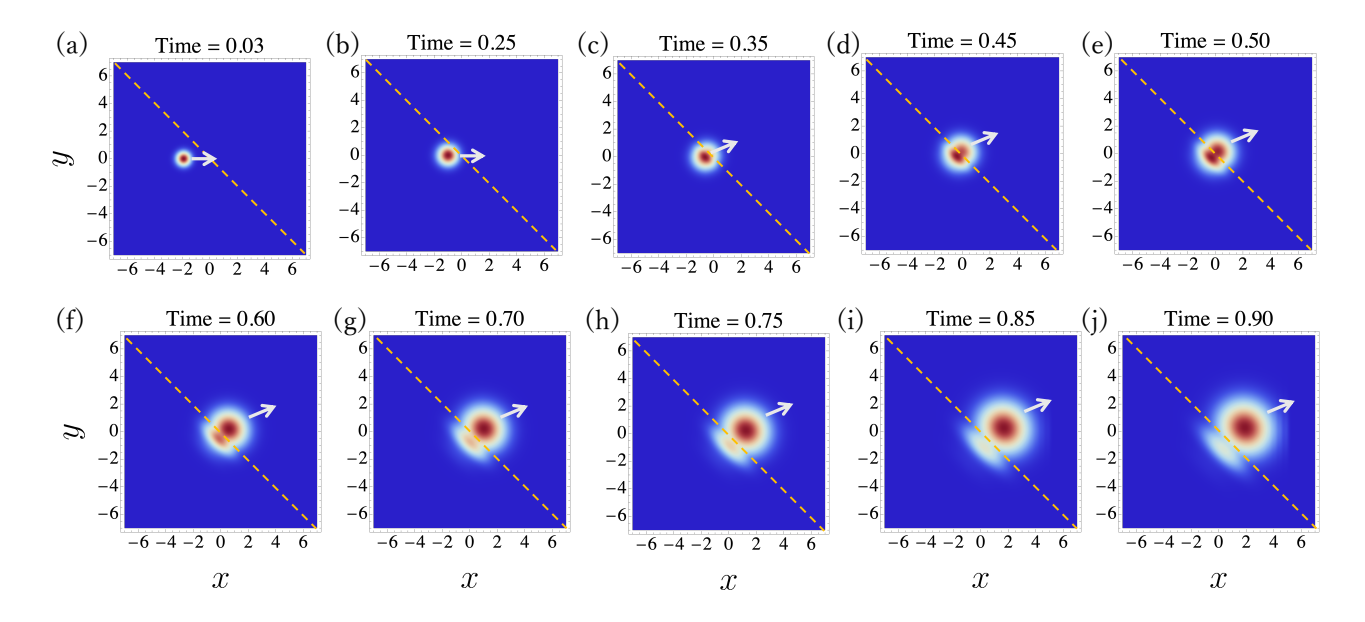


FIG. 3. Time dynamics illustrating the refraction Hall effect. The time evolution of a Gaussian wave packet initially localized at (-2,0) is shown. The packet is assigned an initial momentum along the x-direction, resulting in horizontal propagation prior to interaction with the tilted potential barrier. Upon transmission through the barrier, the wave packet acquires a finite positive momentum component along the y-direction, thereby demonstrating the refraction Hall effect of electrons. The dynamics is computed by numerically solving the time-dependent Schrödinger equation. The dashed line indicates the interface of the potential barrier. The potential takes the value V_0 above the line and vanishes below it. In this case, the barrier is tilted at an angle $\theta = \pi/4$ with respect to the axes, and the barrier strength is $V_0 = -0.5$.

Moreover, by the conservation of energy, we have, $k_{\bar{x}}' = \sqrt{k_{\bar{x}}^2 - 2mV_0/\hbar^2}$. Combining this with the previously derived expression for the transmission probability, we obtain

the total transverse current as

$$\delta I_{Y} = \frac{\hbar^{2}}{m\pi^{2}} \int dk_{\bar{x}} dk_{\bar{y}} \frac{k_{\bar{x}}^{2}}{k_{\bar{x}} + \sqrt{k_{\bar{x}}^{2} - 2mV_{0}/\hbar^{2}}} \times \left(\sqrt{k_{\bar{x}}^{2} - 2mV_{0}/\hbar^{2}} \sin\theta + k_{\bar{y}} \cos\theta\right).$$
 (6)

We now transform to radial coordinates ($\int dk_{\bar{x}} \ dk_{\bar{y}} \rightarrow \int k \ dk \int d\phi$). Assuming the chemical potential bias, $\delta\mu$, is small, we make the approximation, $k^2 \simeq 2m\mu/\hbar^2$. This allows us to simplify the integral, $\int k \ dk = \frac{1}{2} \int d(k^2) \simeq \frac{m\delta\mu}{\hbar^2}$. We finally obtain the differential Hall conductivity, $G(\mu, V_0, \theta) = \delta I_Y/\delta\mu$, as

$$G(\mu, V_0, \theta) = \frac{2m\mu}{\pi^2 \hbar^2} \int d\phi \, \frac{\cos^2(\phi - \theta)}{(\cos(\phi - \theta) + \sqrt{\cos^2(\phi - \theta) - \nu^2})^2} \, \left(\sqrt{\cos^2(\phi - \theta) - \nu^2} \, \sin\theta + \sin(\phi - \theta) \cos\theta \right), \quad (7)$$

where θ is the tilt angle of the potential, and $\nu^2 = V_0^2/\mu^2$. We can verify two limiting cases from Eq. (7). First, in the absence of a potential, $V_0 = 0$, we find $G \sim \int d\phi [\cos{(\phi-\theta)}\sin{\theta} + \sin{(\phi-\theta)}\cos{\theta}]$, which vanishes upon integrating over ϕ . Second, for a potential that is not tilted, $\theta = 0$, we obtain $G \sim \int d\phi \frac{\cos^2{\phi}\sin{\phi}}{(\cos{\phi}+\sqrt{\cos^2{\phi}-\nu^2})^2} = 0$, since the integrand is an odd function of ϕ .

The transverse response, as derived from our analytical

calculations, is presented in Fig. 2. The Hall conductivity is shown as a function of μ . When $\mu < V_0$, no response is observed, as the electrons undergo reflection and are unable to penetrate the potential barrier. However, for $\mu > V_0$, a non-zero G_{XY} is obtained, leading to a finite Hall response in the system, even in the absence of a magnetic field.

Dynamics under the refraction Hall effect— To illustrate the refraction Hall effect, we next consider the dynamical

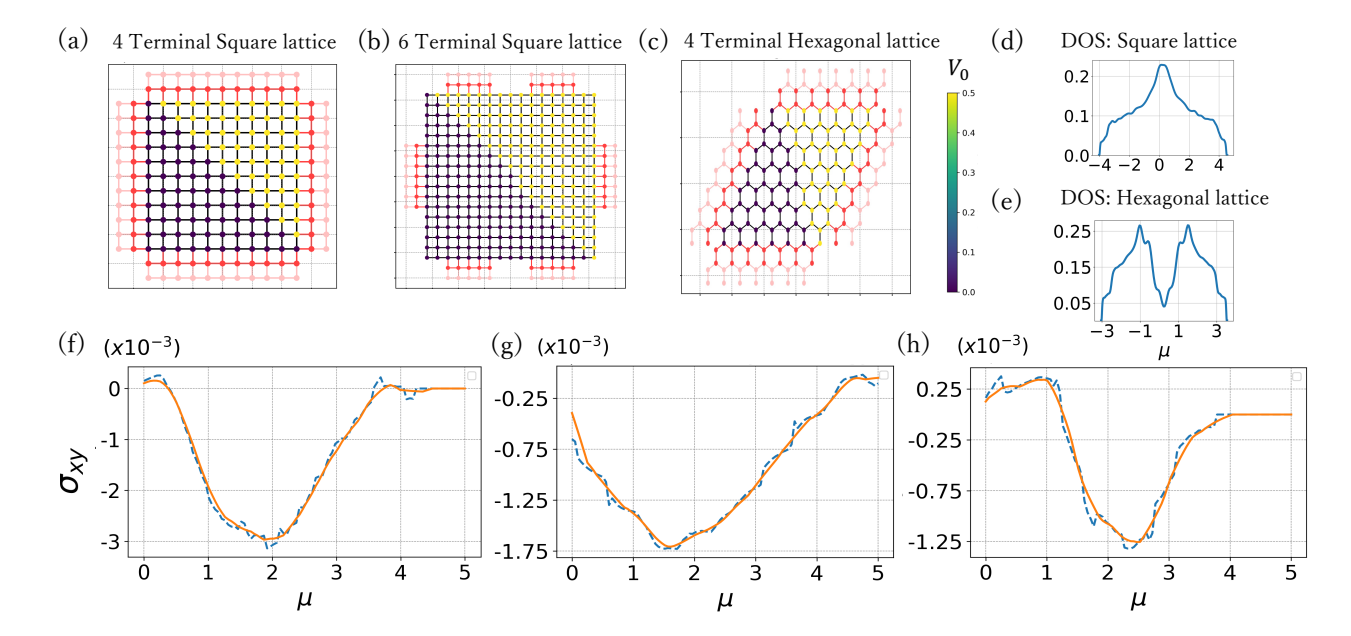


FIG. 4. **Refraction Hall conductivity from lattice simulations.** The upper panels (a)-(c) depict the schematic structure of the simulated device geometries, while the corresponding Hall conductivities are shown in the lower panels (f)-(h). Panels (a) and (f) present results for a four-terminal square lattice; panels (b) and (g) correspond to a six-terminal square lattice; and panels (c) and (h) show a four-terminal hexagonal lattice. In all cases, the potential barrier has a tilt angle of $\theta=0.025$ π and strength $V_0=0.5$. A longitudinal current is applied between the horizontal leads, and the Hall voltage is measured across the vertical leads. The numerical simulations reproduce the analytical trends within the regime of interest. Blue dashed lines denote the moving average of the raw data, while orange curves denote the smoothened profiles. Panels (d) and (e) show the normalized density of states (DOS) with the chemical potential, μ , for the square and hexagonal lattice structures, respectively. All conductivities are expressed in units of e^2/h . Here the lattice dimensions are $L_X=20$, $L_Y=200$ for square lattices and $L_X=20$, $L_Y=400$ for hexagonal lattice geometries.

evolution of a typical refraction Hall setup. We construct a square lattice and engineer a tilted negative potential at an angle $\theta=\pi/4$ for visual clarity. A Gaussian wave packet, initially centered at (-2,0) within the system, is introduced and its time evolution is tracked using the time-dependent Schrödinger equation. The wave packet is initially given a momentum along the x-direction, with no component of momentum in the transverse y-direction.

As depicted in Fig. 3, the wave packet initially propagates horizontally towards the potential barrier. In addition to its motion along the x-direction, the wave packet exhibits a spreading, typical of Gaussian time-evolution. Importantly, when the wave packet encounters the tilted potential barrier, shown by the dashed line, a distinct feature emerges – the wave packet acquires a component of momentum in the transverse y-direction, indicating a clear Hall response. This transverse component is associated with the portion that is refracted into the region with the potential, acquiring a finite momentum along y. Since our simulation uses a negative potential, the electron wavepacket refracts toward the normal.

These observations are in direct agreement with both our analytical calculations and the results obtained from the numerical simulations (detailed in the next section). The emergence of a transverse momentum component from an initially purely longitudinal wave packet provides evidence of the Hall response in this system, driven by refraction at the tilted po-

tential barrier. The dynamics observed confirm the validity of our analytical framework and illustrate how such a Hall effect can arise due to the interaction of the wave packet with a tilted potential, *without* the need for a magnetic field.

Refraction Hall conductivity for lattice models- To further complement our analytical results, we next simulate a "refraction Hall" geometry. We examine several device geometries of direct experimental feasibility using the Kwant simulation package [36], and compute the Hall response by employing scattering matrix calculations. The different geometries are schematically illustrated in the upper panels of Fig. 4 (a)-(c). We consider square lattice geometries with four- and sixterminal geometries, along with the hexagonal lattice geometry. For each geometry, we model the scattering region, described by a nearest-neighbor tight-binding model. The tilted potential is incorporated within the scattering region, with a constant value $V_0 = 0.5$, chosen to closely mirror the conditions of our analytical calculations. The leads, shown in red in Fig. 4, are attached to the scattering region and extend to infinity. The input current is constrained to flow from the left to the right terminals in all cases, while the Hall voltage is measured between the upper and lower terminals, enabling the calculation of the Hall conductivity, σ_{xy} . This is shown in the lower panels of Fig. 4 (f)-(h). The conductivity results, represented by blue dashed lines in these panels, are computed using a moving average, while the orange curves are the smoothed profiles to highlight the general trend.

In all of the simulated geometries, a non-zero Hall response is observed as a function of the Fermi energy, μ , and the magnitude of this response is of the same order as predicted by our analytical calculations. While an exact match between the analytical and simulated results is not expected, the general agreement establishes the validity of our proposed effect. Our theory assumes a quadratic-dispersion electron model for simplicity, whereas the numerical simulations use a more realistic tight-binding lattice model, which accounts for additional effects such as the band structure. One noticeable deviation from the theoretical predictions arises when the Hall conductivity becomes zero after a certain value of μ . This is simply due to the density of states being non-zero only in a finite energy window, as illustrated in Fig. 4 (d)-(e), for both square and hexagonal lattice geometries. When μ lies outside this energy window, no states are available for conduction, causing the Hall response to vanish. However, within this energy window, a non-zero Hall response is clearly observed, confirming the viability of the proposed geometries for experimental realization. Overall, these simulations corroborate our analytical predictions and suggest that the refraction Hall response is a robust feature, clearly observed across different lattice models. Finally, we note that our analysis assumes ballistic transport. Graphene, with its hallmark hexagonal lattice, is well-known to exhibit ballistic transport features [37-40], making it a promising platform for the experimental realization of our predicted refraction Hall effect.

Summary and outlook- In summary, we proposed and developed a new Hall-like response that arises without an external magnetic field or breaking of time-reversal symmetry. We demonstrated that a tilted potential interface induces a refraction-like behavior of electron wave packets, producing a finite transverse current and a Hall conductivity. This refraction Hall effect emerges purely from the geometric features of the potential landscape and represents a fundamentally distinct mechanism for generating transverse transport in time-reversal-invariant systems. Our analytical framework, supported by numerical simulations on different lattice models and device geometries, consistently captures the essential features of the effect. The real-time wave packet dynamics further provides a direct visualization of this effect, revealing its geometric origin and a robustness of the transverse response. Our findings demonstrate that geometric control of potential barriers offers a powerful route to manipulate Hall-like transport in mesoscopic systems. Tilted potential interfaces may occur naturally in certain experimental settings or can be engineered by substrates or structural asymmetries that induce spatially varying onsite potentials [41–51]. Overall, our results open as-yet-unexplored avenues for designing devices that exploit geometric effects to harness unconventional Hall responses.

Acknowledgments— R.S. is supported by the Prime

Minister's Research Fellowship (PMRF). A.N. acknowledges DST CRG grant (CRG/2023/000114) for support. D.S. thanks SERB, India for support through the project JBR/2020/000043.

- * ronikasarkar@iisc.ac.in
- arka.bandyopadhyay@uni-wuerzburg.de
- [‡] awadhesh@iisc.ac.in
- § diptiman@iisc.ac.in
- R. Takahashi and S. Murakami, Gapless interface states between topological insulators with opposite dirac velocities, Phys. Rev. Lett. 107, 166805 (2011).
- [2] R. R. Biswas and A. V. Balatsky, Scattering from surface step edges in strong topological insulators, Phys. Rev. B 83, 075439 (2011).
- [3] D. Sen and O. Deb, Junction between surfaces of two topological insulators, Phys. Rev. B **85**, 245402 (2012).
- [4] A. Soori, O. Deb, K. Sengupta, and D. Sen, Transport across a junction of topological insulators and a superconductor, Phys. Rev. B 87, 245435 (2013).
- [5] E. H. Hall, On a new action of the magnet on electric currents, American Journal of Mathematics 2, 287 (1879).
- [6] N. Nagaosa, J. Sinova, S. Onoda, A. H. MacDonald, and N. P. Ong, Anomalous hall effect, Rev. Mod. Phys. 82, 1539 (2010).
- [7] T. Jungwirth, Q. Niu, and A. H. MacDonald, Anomalous hall effect in ferromagnetic semiconductors, Phys. Rev. Lett. 88, 207208 (2002).
- [8] S. Nakatsuji, N. Kiyohara, and T. Higo, Large anomalous hall effect in a non-collinear antiferromagnet at room temperature, Nature 527, 212 (2015).
- [9] J. Sinova, S. O. Valenzuela, J. Wunderlich, C. H. Back, and T. Jungwirth, Spin hall effects, Rev. Mod. Phys. 87, 1213 (2015)
- [10] J. E. Hirsch, Spin hall effect, Phys. Rev. Lett. 83, 1834 (1999).
- [11] A. Hoffmann, Spin hall effects in metals, IEEE Transactions on Magnetics 49, 5172 (2013).
- [12] S. O. Valenzuela and M. Tinkham, Direct electronic measurement of the spin hall effect, Nature 442, 176 (2006).
- [13] Y. K. Kato, R. C. Myers, A. C. Gossard, and D. D. Awschalom, Observation of the spin hall effect in semiconductors, Science 306, 1910 (2004).
- [14] K. v. Klitzing, G. Dorda, and M. Pepper, New method for high-accuracy determination of the fine-structure constant based on quantized hall resistance, Phys. Rev. Lett. 45, 494 (1980).
- [15] R. E. Prange and S. M. Girvin, *The quantum Hall effect* (Springer, New York, 1987).
- [16] M. Stone, Quantum Hall Effect (World Scientific, Singapore, 1992).
- [17] H. L. Stormer, D. C. Tsui, and A. C. Gossard, The fractional quantum hall effect, Rev. Mod. Phys. 71, S298 (1999).
- [18] G. Moore and N. Read, Nonabelions in the fractional quantum hall effect, Nuclear Physics B 360, 362 (1991).
- [19] K. I. Bolotin, F. Ghahari, M. D. Shulman, H. L. Stormer, and P. Kim, Observation of the fractional quantum hall effect in graphene, Nature 462, 196 (2009).
- [20] B. A. Bernevig and S.-C. Zhang, Quantum spin hall effect, Phys. Rev. Lett. 96, 106802 (2006).
- [21] C. L. Kane and E. J. Mele, Quantum spin hall effect in graphene, Phys. Rev. Lett. 95, 226801 (2005).
- [22] X.-L. Qi and S.-C. Zhang, The quantum spin hall effect and

- topological insulators, Physics Today 63, 33 (2010).
- [23] F. D. M. Haldane, Model for a quantum hall effect without landau levels: Condensed-matter realization of the "parity anomaly", Phys. Rev. Lett. 61, 2015 (1988).
- [24] C.-Z. Chang, J. Zhang, X. Feng, J. Shen, Z. Zhang, M. Guo, K. Li, Y. Ou, P. Wei, L.-L. Wang, et al., Experimental observation of the quantum anomalous hall effect in a magnetic topological insulator, Science 340, 167 (2013).
- [25] C.-X. Liu, S.-C. Zhang, and X.-L. Qi, The quantum anomalous hall effect: theory and experiment, Annual Review of Condensed Matter Physics 7, 301 (2016).
- [26] H. Katsura, N. Nagaosa, and P. A. Lee, Theory of the thermal hall effect in quantum magnets, Phys. Rev. Lett. 104, 066403 (2010).
- [27] M. Banerjee, M. Heiblum, V. Umansky, D. E. Feldman, Y. Oreg, and A. Stern, Observation of half-integer thermal hall conductance, Nature 559, 205 (2018).
- [28] Y. Kasahara, T. Ohnishi, Y. Mizukami, O. Tanaka, S. Ma, K. Sugii, N. Kurita, H. Tanaka, J. Nasu, Y. Motome, *et al.*, Majorana quantization and half-integer thermal quantum hall effect in a kitaev spin liquid, Nature 559, 227 (2018).
- [29] I. Sodemann and L. Fu, Quantum nonlinear hall effect induced by berry curvature dipole in time-reversal invariant materials, Phys. Rev. Lett. 115, 216806 (2015).
- [30] Z. Du, H.-Z. Lu, and X. Xie, Nonlinear hall effects, Nature Reviews Physics 3, 744 (2021).
- [31] C. Ortix, Nonlinear hall effect with time-reversal symmetry: Theory and material realizations, Advanced Quantum Technologies 4, 2100056 (2021).
- [32] A. Bandyopadhyay, N. B. Joseph, and A. Narayan, Non-linear hall effects: Mechanisms and materials, Materials Today Electronics 8, 100101 (2024).
- [33] M. Papaj and L. Fu, Magnus hall effect, Phys. Rev. Lett. 123, 216802 (2019).
- [34] D. Mandal, K. Das, and A. Agarwal, Magnus nernst and thermal hall effect, Phys. Rev. B 102, 205414 (2020).
- [35] L. F. O. Costa, R. Franco, and V. Cardoso, Gravitational magnus effect, Phys. Rev. D 98, 024026 (2018).
- [36] C. W. Groth, M. Wimmer, A. R. Akhmerov, and X. Waintal, Kwant: a software package for quantum transport, New Journal of Physics 16, 063065 (2014).
- [37] X. Du, I. Skachko, A. Barker, and E. Y. Andrei, Approaching ballistic transport in suspended graphene, Nature Nanotechnology 3, 491 (2008).
- [38] A. S. Mayorov, R. V. Gorbachev, S. V. Morozov, L. Britnell, R. Jalil, L. A. Ponomarenko, P. Blake, K. S. Novoselov,

- K. Watanabe, T. Taniguchi, and A. K. Geim, Micrometer-scale ballistic transport in encapsulated graphene at room temperature, Nano Letters 11, 2396 (2011).
- [39] J. Baringhaus, M. Ruan, F. Edler, A. Tejeda, M. Sicot, A. Taleb-Ibrahimi, A.-P. Li, Z. Jiang, E. H. Conrad, C. Berger, et al., Exceptional ballistic transport in epitaxial graphene nanoribbons, Nature 506, 349 (2014).
- [40] S. Chen, Z. Han, M. M. Elahi, K. M. Habib, L. Wang, B. Wen, Y. Gao, T. Taniguchi, K. Watanabe, J. Hone, *et al.*, Electron optics with p-n junctions in ballistic graphene, Science 353, 1522 (2016).
- [41] P. Muggli, S. Lee, T. Katsouleas, R. Assmann, F.-J. Decker, M. J. Hogan, R. Iverson, P. Raimondi, R. H. Siemann, D. Walz, et al., Refraction of a particle beam, Nature 411, 43 (2001).
- [42] J. Repp, G. Meyer, and K.-H. Rieder, Snell's law for surface electrons: refraction of an electron gas imaged in real space, Physical Review Letters 92, 036803 (2004).
- [43] V. V. Cheianov, V. Fal'ko, and B. L. Altshuler, The focusing of electron flow and a veselago lens in graphene p-n junctions, Science 315, 1252–1255 (2007).
- [44] T. Low and J. Appenzeller, Electronic transport properties of a tilted graphene p-n junction, Physical Review B—Condensed Matter and Materials Physics 80, 155406 (2009).
- [45] A. G. Moghaddam and M. Zareyan, Graphene-based electronic spin lenses, Physical Review Letters 105, 146803 (2010).
- [46] J.-H. Gao, J. Yuan, W.-Q. Chen, Y. Zhou, and F.-C. Zhang, Giant mesoscopic spin hall effect on the surface of topological insulator, Physical Review Letters 106, 057205 (2011).
- [47] G.-H. Lee, G.-H. Park, and H.-J. Lee, Observation of negative refraction of dirac fermions in graphene, Nature Physics 11, 925–929 (2015).
- [48] C. Baeumer, D. Saldana-Greco, J. M. P. Martirez, A. M. Rappe, M. Shim, and L. W. Martin, Ferroelectrically driven spatial carrier density modulation in graphene, Nature Communications 6, 6136 (2015).
- [49] J. Li, K. Wang, K. J. McFaul, Z. Zern, Y. Ren, K. Watanabe, T. Taniguchi, Z. Qiao, and J. Zhu, Gate-controlled topological conducting channels in bilayer graphene, Nature Nanotechnology 11, 1060 (2016).
- [50] M.-H. Liu, C. Gorini, and K. Richter, Creating and steering highly directional electron beams in graphene, Physical Review Letters 118, 066801 (2017).
- [51] H. Ye, C. Qin, S. Wang, L. Zhao, W. Liu, B. Wang, S. Longhi, and P. Lu, Reconfigurable refraction manipulation at synthetic temporal interfaces with scalar and vector gauge potentials, Proceedings of the National Academy of Sciences 120, e2300860120 (2023).